

## Research Article

# Alumina and Hafnia ALD Layers for a Niobium-Doped Titanium Oxide Photoanode

Naji Al Dahoudi,<sup>1,2</sup> Qifeng Zhang,<sup>1</sup> and Guozhong Cao<sup>1</sup>

<sup>1</sup>Department of Materials Science and Engineering, University of Washington, Seattle, WA 98195, USA

<sup>2</sup>Physics Department, Al-Azhar University-Gaza, P.O. Box 1277, Gaza, Palestine

Correspondence should be addressed to Naji Al Dahoudi, naji@alazhar.edu.ps

Received 13 November 2012; Accepted 18 December 2012

Academic Editor: Sudhakar Shet

Copyright © 2012 Naji Al Dahoudi et al. This is an open access article distributed under the Creative Commons Attribution License, which permits unrestricted use, distribution, and reproduction in any medium, provided the original work is properly cited.

Niobium-doped titanium dioxide (TiO<sub>2</sub>) nanoparticles were used as a photoanode in dye-sensitized solar cells (DSCs). They showed a high photocurrent density due to their higher conductivity; however, a low open-circuit voltage was exhibited due to the back-reaction of photogenerated electrons. Atomic layer deposition is a useful technique to form a conformal ultrathin layer of Al<sub>2</sub>O<sub>3</sub> and HfO, which act as an energy barrier to suppress the back electrons from reaching the redox medium. This resulted in an increase of the open-circuit voltage and therefore led to higher performance. HfO showed an improvement of the light-to-current conversion efficiency by 74%, higher than the 21% enhancement obtained by utilizing Al<sub>2</sub>O<sub>3</sub> layers.

## 1. Introduction

The world is in urgent quest of seeking alternative renewable energy resources. Because of their low-cost materials and their simple elaboration of manufacturing, dye-sensitized solar cells [1–5] are considered as a promising candidate to replace the commercial silicon solar cells [6–8]. Titanium oxide is one of the extremely favorable materials [9] for the working electrode (photoanode) of DSCs. The control of their morphological properties, structure, and the kinetic transport of the charge carriers have a significant impact of their performance in the DSSCs. Using metal ions as dopants has a significant effect on the electrical properties of TiO<sub>2</sub>. This doping leads to significant changes of electrical conductivity, shifting of Fermi level potential, particle aggregation, charge transfer kinetics, and dye absorption characteristics of TiO<sub>2</sub> [10]. Ko et al. [11] have found remarkable enhancement by doping the TiO<sub>2</sub> with aluminum and tungsten.

However, many reports have suggested that the performance of DSCs at the optimized level of metal ions doping into TiO<sub>2</sub> relates mainly the tuning of the flat band of TiO<sub>2</sub>. Lü et al. [12] synthesized a well-crystalline niobium (Nb) doped anatase TiO<sub>2</sub> (Nb : TiO<sub>2</sub>) and investigated its effect on the performance of DSSCs. It was revealed that Nb doping

had positive effect on the short-circuit current with positive shift of the flat band potential. Doping of titanium oxide by metal ions may elevate the electron hole pair production, however, may create more trapping sites that affect the performance of dye-sensitized solar cells. Charge recombination occurs at the interface between the working electrode and the dye/electrolyte interfaces, where photogenerated electrons in the porous electrode tend to recombine with either the oxidized dye or the oxidized species in electrolyte, thereby reducing the open-circuit voltage. One effective approach for impeding charge recombination is to apply the porous electrode/dye interface with a thin insulating metal oxide layer, which impedes charge recombination by forming an energy barrier for charge transport at the interface. Since the insulating layer impedes both charge recombination and electron injection, the thickness of the insulating layer should be optimized that does not affect the electron injection through the photoanode. So, atomic layer deposition (ALD) is an effective technique to deposit ultrathin layer with controllable thickness, where no other deposition technique can achieve the conformality as that done by the ALD on high-aspect structures [13].

In this work niobium doped titanium oxide nanoparticles were employed to fabricate a photoanode film of DSCs.

To increase the open circuit voltage of the cell, atomic deposited layers of  $\text{Al}_2\text{O}_3$  and  $\text{HfO}$  were utilized to form conformal insulating layers to suppress the charge recombination. The thickness of the coating layers was optimized to achieve the best performance.

## 2. Experimental Work

Nanoparticles of undoped  $\text{TiO}_2$  for preparing the photoanode film were obtained through hydrothermal treatment of  $\text{TiO}_2$  sol, as previously reported. The Nb-doped  $\text{TiO}_2$  was obtained by a cohydrolysis of Ti and Nb precursors (e.g., titanium isopropoxide and niobium ethoxide, resp.) in an atomic ratio of 95:5. The precursor solution underwent a hydrothermal growth at  $200^\circ\text{C}$  for 5 h. The resultant precipitate was washed with water and ethanol for several times, dried at  $90^\circ\text{C}$ , and ground to fine powder for use.

Typically, 0.1 g of Nb:TiO<sub>2</sub> nanopowder is wetted and grinded by using 0.3 g of 15 wt.% aqueous polyethylene glycol (PEG20T) in a mortar for 5 minutes until a homogeneous viscous paste was formed. The Nb:TiO<sub>2</sub> paste was deposited onto FTO glass substrates using the doctor blading technique to form a  $(14\text{--}16) \pm 2 \mu\text{m}$  thick film. The obtained films were dried for 30 min at  $100^\circ\text{C}$  and then heated in air up to  $450^\circ\text{C}$  for 60 min.

## 3. ALD of Alumina and Hafnia

The Nb:TiO<sub>2</sub> films were then treated by atomic layer deposition (Oxford OpAL System) of  $\text{Al}_2\text{O}_3$  and  $\text{HfO}$  for 0, 5, 10, 15, and 20 cycles, respectively. The deposition temperature was kept at  $25^\circ\text{C}$  for the precursor and an argon gas was used as a carrier gas to deliver the precursor effectively. The substrate temperature was kept at  $180^\circ\text{C}$  during the ALD process. The deposition rate was 0.8 and  $0.5 \text{ \AA}$  per cycle for  $\text{Al}_2\text{O}_3$  and  $\text{HfO}$ , respectively. After the ALD process, the coated film was reannealed at  $450^\circ\text{C}$ .

## 4. Cell Assembly and Characterization

All the films were sensitized by immersing in a 0.5 mM ruthenium-based N719 dye solution for 24 h, then rinsed with ethanol and dried in air at RT. A Pt-coated silicon substrate was used as the counter electrode, and an iodide-based solution, consisting of 0.6 M tetrabutylammonium iodide, 0.1 M lithium iodide, 0.1 M iodine, and 0.5 M 4-*tert*-butylpyridine in acetonitrile, was used as the liquid electrolyte. Photovoltaic properties of each solar cell were characterized using simulated AM 1.5 sunlight illumination with an output power of  $100 \text{ mW/cm}^2$ . An ultraviolet solar simulator (Model 16S, Solar Light Co., Philadelphia, PA, USA) with a 200 W xenon lamp power supply (Model XPS 200, Solar Light Co., Philadelphia, PA, USA) was used as the light source, and a semiconductor parameter analyzer (4155A, Hewlett-Packard, Japan) was used to measure the current and voltage. The  $J$ - $V$  measurement was repeated three times and the average results were reported. The electrochemical impedance spectroscopy (EIS) was carried

out through the Solartron 1287A coupling with the Solartron 1260 FRA/impedance analyzer to investigate electronic and ionic processes in DSCs.

The morphology of the photoanode surfaces was characterized by scanning electron microscopy (SEM, JEOL JSM-7000).

To measure the adsorbed N3 dye amount on the films, the dye was desorbed by immersing dye-sensitized films in a solution containing 0.1 M NaOH in water and ethanol (1:1, v/v). An ultraviolet-visible-near infrared spectrophotometer (UV-VIS-NIR, Perkin Elmer Lambda 900) was employed to measure the dye concentration of the desorbed-dye solution.

## 5. Results and Discussions

The  $J$ - $V$  curves and the performance characteristic values ( $J_{sc}$ ,  $V_{oc}$ ,  $\eta$ , and  $ff$ ) for the DSCs based on the Nb-TiO<sub>2</sub> photoanode before and after the atomic deposition of alumina and hafnia layers are depicted on Figures 1(a) and 1(b) and summarized in Table 1. The niobium-doped titanium oxide photoanode showed a relatively high photocurrent density ( $14.25 \text{ mA/cm}^2$ ) corresponding to relatively high dye loading ( $2.22 \times 10^{-7} \text{ mol/cm}^2$ ), but a low open-circuit voltage (547 mV) which result in an efficiency of 2.93%. The low open circuit voltage is explained as a result of the high rate of charge recombination, where photogenerated electrons in the porous electrode tend to recombine with either the oxidized dye or the oxidized species in the electrolyte, thereby reducing the open-circuit voltage [14]. The deposition of atomic layers of alumina resulted in an increase of the open-circuit voltage up to 623 mV after 20 cycles and an increase of the photocurrent density up to  $18.53 \text{ mA/cm}^2$  after 15 cycles. The increase in photocurrent, and hence efficiency, is likely to arise from the improved connectivity of the nanoparticles composed the photoanode, where no perceptible change can be observed in the dye loading, but presents a reduction in carrier recombination. The alumina layers showed a more effective suppression of the charge recombination by increasing the thickness of the layers which resulted in an increase of the open circuit voltage up to 14% and the overall efficiency up to 21%. Beyond 15 cycles of ALD of alumina, a decrease in the photocurrent density was founded, which is attributed to the low efficiency of the electron transport due to too much thickness of the coating layer.

On the other hand, using hafnium oxide as a passivation layer of the Nb-doped titania nanoparticles exhibited much more enhancement compared with the utilization of alumina layer as shown in Figure 1(b). The open-circuit voltage increased gradually from 547 mV to 675 mV by increasing the number of the ALD hafnia layers up to 15 cycles. The photocurrent density increased up to  $16.43 \text{ mA/cm}^2$  after 5 cycles followed by minimal drop for the 10 cycles sample and further drop down to  $14.4 \text{ mA/cm}^2$  for the 15 cycles sample. This behavior is correlated with the dye loading as shown in Table 1. So, by incorporating 10 cycles of ultrathin hafnia layers, the best performance with overall efficiency of 5.12% was achieved, which exemplifies an improvement of

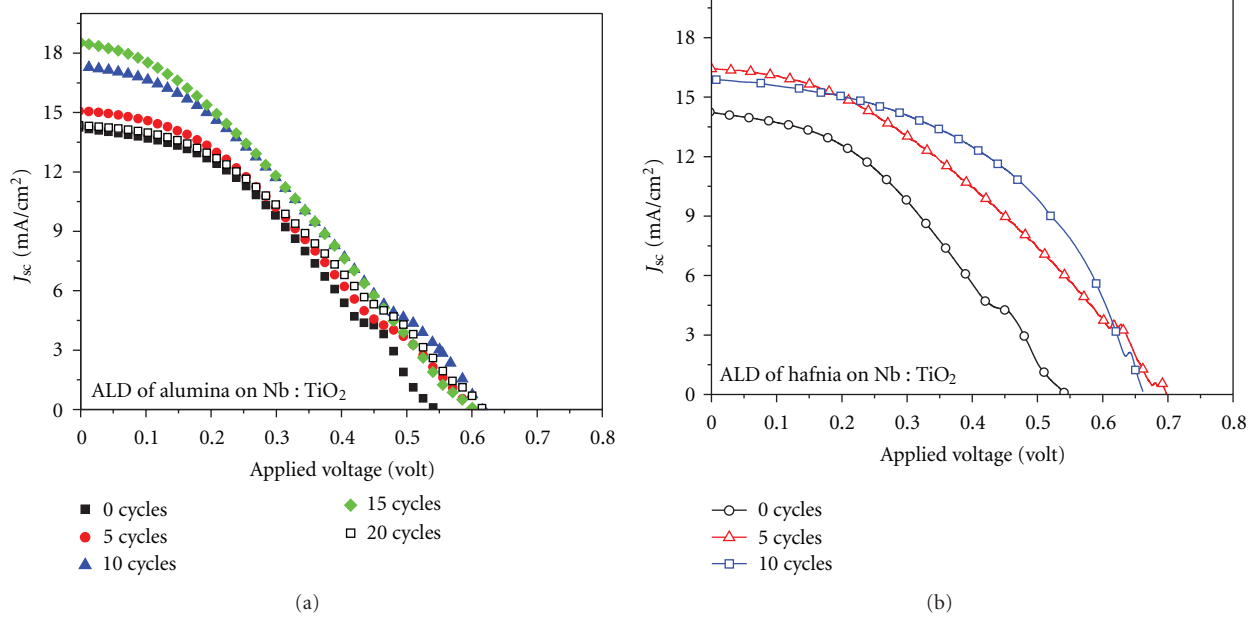


FIGURE 1: The  $J$ - $V$  curves for DSCs composed of ALD of alumina on Nb:TiO<sub>2</sub> photoanode (a) and of hafnia-coated one (b) treated with different cycles.

TABLE 1: The DSC performance parameters for alumina and hafnia ALD Nb:TiO<sub>2</sub> photoanode coated with different cycles.

	$J_{sc}$ (mA/cm <sup>2</sup> )		$V_{oc}$ ( $<\pm 0.01$ Volt)		$\eta$ (%)		FF ( $<\pm 0.01$ )		Dye loading $\times 10^{-7}$ (mol/cm <sup>2</sup> )	
	Al <sub>2</sub> O <sub>3</sub>	HfO	Al <sub>2</sub> O <sub>3</sub>	HfO	Al <sub>2</sub> O <sub>3</sub>	HfO	Al <sub>2</sub> O <sub>3</sub>	HfO	Al <sub>2</sub> O <sub>3</sub>	HfO
0 cycles	14.25 $\pm$ 0.15	14.25 $\pm$ 0.11	547	547	2.93 $\pm$ 0.04	2.93 $\pm$ 0.04	0.38	0.38	2.20	2.20
5 cycles	15.1 $\pm$ 0.17	16.43 $\pm$ 0.08	600	698	3.06 $\pm$ 0.05	4.16 $\pm$ 0.03	0.34	0.36	2.29	2.35
10 cycles	17.3 $\pm$ 0.14	15.9 $\pm$ 0.15	616	663	3.5 $\pm$ 0.07	5.12 $\pm$ 0.06	0.33	0.45	2.26	2.27
15 cycles	18.53 $\pm$ 0.16	14.4 $\pm$ 0.11	610	675	3.55 $\pm$ 0.03	3.72 $\pm$ 0.04	0.31	0.38	2.16	1.77
20 cycles	14.4 $\pm$ 0.2	—	623	—	3.1 $\pm$ 0.06	—	0.35	—	1.89	—

74%. Such an enhancement of the performance explained the improvement of the fill factor. This is attributed to better electron transport via the interfaces, which means that the diffuse of the hafnia phase through the photoanode network is efficient and can be demonstrated as a conformal buffering coating to suppress the leakage current. Both alumina and hafnia layers have a higher conduction band edge from niobium-doped titanium oxide, which act as a blocking layer of the back electrons [15].

## 6. Structural Properties

XRD pattern for the layers did not show any traces for alumina or hafnia, as the expected XRD is not sensitive for this ultrathin layer. It is very likely that we have an amorphous ALD coating, or with very poor crystallinity. The surface morphology of the niobium-doped titanium oxide is depicted in Figure 2(a) using different magnification. The film exhibited a mesoporous structure, which led to better dye loading. Figures 2(b) and 2(c)

exhibited the surface morphology of the niobium-doped titanium oxide layer after 10 cycles of ALD of alumina and hafnia, respectively. The ALD layers of alumina and hafnia formed a homogenous conformal coverage on the surface of Nb:TiO<sub>2</sub> nanoparticles and inside the mesoporous structure enhancing the coalescence between the nanocrystalline nanoparticles making them closer, which may introduce favorable path for electron transport through the photoanode layer. In addition, the porous structure of the layer is still retained as shown in Figure 2(c), which preserves the high dye loading ability. So, the ALD hafnia improved the connectivity of the emerged nanoparticles with enhanced blocking layer against the leakage current, while retaining the high dye loading of the photoanode as shown in Table 1. The composition of the surface of the layer, which was determined by the EDX, exhibited the existence of the elements K-lines of aluminum, niobium, and titanium referred to the L-spectrum (see the inset in Figure 2(b)). However, it is difficult to argue that a doping of aluminum or hafnium is expected to

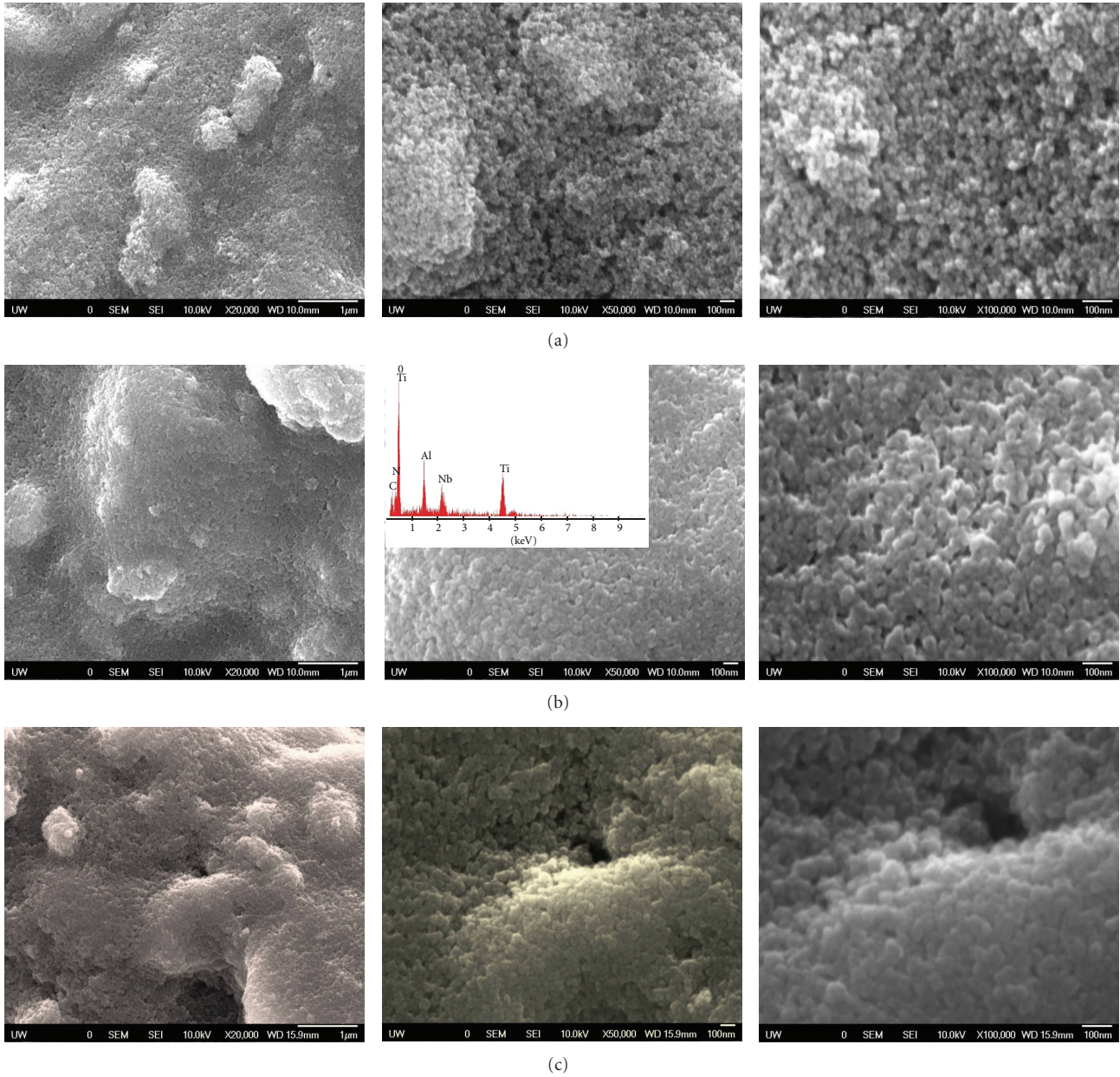


FIGURE 2: SEM images of the surface of (a) uncoated Nb : TiO<sub>2</sub> films, for Nb : TiO<sub>2</sub> layer treated with 10 cycle of ALD of (b) alumina and (c) hafnia. The index of (b) showed the EDX spectrum of the layer.

take place. The SEM images revealed a coverage effect more likely.

## 7. Electrochemical Impedance Spectroscopy (EIS)

Figures 3(a) and 3(b) exhibit the typical electrochemical impedance spectroscopy (EIS) Nyquist plots for the assembled DSCs made of ALD alumina and hafnia photoanode, respectively. Two semicircles is appeared, where the smallest one in the high-frequency range represents the

electrochemical reaction at the counter electrode and the largest one represents the charge transfer resistance at the electrolyte/dye/metal oxide interfaces. The diameter of the semicircle of the ALD alumina and hafnia photoanode is larger than that of the uncoated one, which means that the charge transfer resistance increased by the deposition of alumina and hafnia layers over the surface of the nanoparticles. The charge transfer resistance increased by increasing the number of cycles, where the different thickness of the blocking layers may be the major factor of such behavior. The peak of the semicircle in the midfrequency range in the Nyquist plot is correlated with the reaction rate

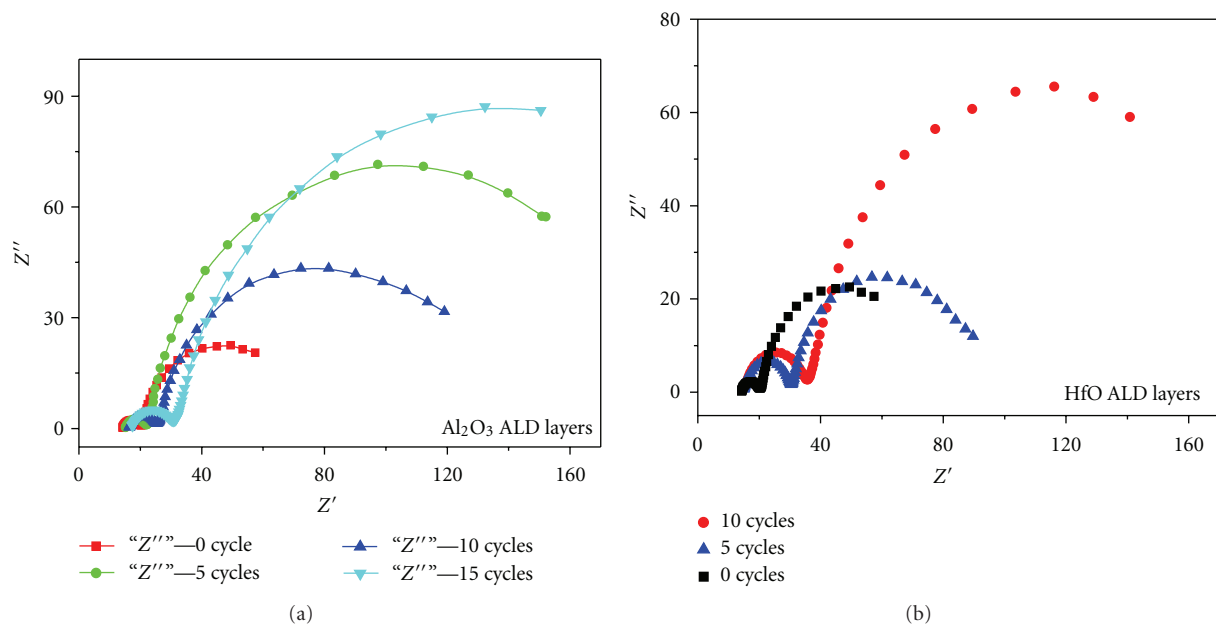


FIGURE 3: EIS spectra showing the Nyquist plots of the alumina ALD layers on Nb:TiO<sub>2</sub> DSC (a) and hafnia ALD layers on Nb:TiO<sub>2</sub> (b) for different cycles.

constant for the recombination process. The shift to higher frequency means a longer life-time is obtained, which results in higher performance of the DSCs.

## 8. Conclusion

Niobium-doped titanium oxide nanoparticulate photoanode in DSC showed a high photocurrent density due to its higher conductivity; however, a low open-circuit voltage is exhibited due to the higher recombination rate. Depositing conformal ultrathin atomic layers of Al<sub>2</sub>O<sub>3</sub> and HfO can suppress the back electrons from reaching the redox medium, which results in an increase of the open-circuit voltage and therefore lead to higher performance. HfO showed an improvement of the light-to-current conversion efficiency by 74%, higher than the 21% enhancement obtained by utilizing Al<sub>2</sub>O<sub>3</sub> layer.

## Conflict of Interests

The authors declare that they have no conflict of interests to disclose. Potential conflicts do not exist.

## Acknowledgments

N. Al Dahoudi would like to acknowledge the Council for International Exchange of Scholars (CIES) for their Fulbright Scholarship. This work is supported in part by the US Department of Energy, Office of Basic Energy Sciences, Division of Materials Sciences, under Award no. DE-FG02-07ER46467 (Q. Zhang), the National Science Foundation (DMR 1035196, DMR-0605159, and CMMI-1030048), and

the Royalty Research Fund (RRF) from the Office of Research at the University of Washington.

## References

- [1] R. D. McConnell, "Assessment of the dye-sensitized solar cell," *Renewable and Sustainable Energy Reviews*, vol. 6, no. 3, pp. 273–295, 2002.
- [2] B. O'Regan and M. Grätzel, "A low-cost, high-efficiency solar cell based on dye-sensitized colloidal TiO<sub>2</sub> films," *Nature*, vol. 353, no. 6346, pp. 737–740, 1991.
- [3] Y. Chiba, A. Islam, Y. Atanabe, R. Komiya, N. Koide, and L.Y. Han, "Dye-sensitized solar cells with conversion efficiency of 11.1%," *Japanese Journal of Applied Physics*, vol. 45, supplement 2, pp. L638–L640, 2006.
- [4] A. Yella, H.-W. Lee, H. N. Tsao et al., "Porphyrin-sensitized solar cells with cobalt (II/III)-based redox electrolyte exceed 12 percent efficiency," *Science*, vol. 334, no. 6056, pp. 629–634, 2011.
- [5] Q. Zhang and G. Cao, "Nanostructured photoelectrodes for dye-sensitized solar cells," *Nano Today*, vol. 6, no. 1, pp. 91–109, 2011.
- [6] A. G. Aberla, T. Lauinger, and R. Hezel, "Remote PECVD silicon—a key technology for the crystalline silicon PV industry of the 21st century?" in *Proceedings of the 14th European Photovoltaic Solar Energy Conference*, pp. 684–689, H. S. Stephens & Associates, 1997.
- [7] T. Saga, "Advances in crystalline silicon solar cell technology for industrial mass production," *NPG Asia Materials*, vol. 2, pp. 96–102, 2010.
- [8] B. Lim, S. Hermann, K. Bothe, J. Schmidt, and R. Brendel, "Permanent deactivation of the boron-oxygen recombination center in silicon solar cells," in *Proceedings of the 23rd European Photovoltaic Solar Energy Conference*, p. 1018, 2008.
- [9] U. Diebold, "The surface science of titanium dioxide," *Surface Science Reports*, vol. 48, no. 5–8, pp. 53–229, 2003.

- [10] J.-J. Lee, M. Rahman, S. Sarker et al., *Metal Oxides and Their Composites for the Photoelectrode of Dye Sensitized Solar Cells*, *Advances in Composite Materials for Medicine and Nanotechnology*, InTech, 2011.
- [11] K. H. Ko, Y. C. Lee, and Y. J. Jung, "Enhanced efficiency of dye-sensitized TiO<sub>2</sub> solar cells (DSSC) by doping of metal ions," *Journal of Colloid and Interface Science*, vol. 283, no. 2, pp. 482–487, 2005.
- [12] X. Lü, X. Mou, J. Wu et al., "Improved-Performance Dye-Sensitized solar cells using Nb-Doped TiO<sub>2</sub> electrodes: efficient electron Injection and transfer," *Advanced Functional Materials*, vol. 20, no. 3, pp. 509–515, 2010.
- [13] S. M. George, "Atomic layer deposition: an overview," *Chemical Reviews*, vol. 110, no. 1, pp. 111–131, 2010.
- [14] C. Lin, F.-Y. Tsai, M.-H. Lee, C.-H. Lee, T.-C. Tien, and L.-P. Wang, "Enhanced performance of dye-sensitized solar cells by an Al<sub>2</sub>O<sub>3</sub> charge-recombination barrier formed by low-temperature atomic layer deposition," *Journal of Materials Chemistry*, vol. 19, no. 19, pp. 2999–3003, 2009.
- [15] V. Ganapathy, B. Karunakaran, and S.-W. Rhee, "Improved performance of dye-sensitized solar cells with TiO<sub>2</sub>/alumina core-shell formation using atomic layer deposition," *Journal of Power Sources*, vol. 195, no. 15, pp. 5138–5143, 2010.



**Hindawi**

Submit your manuscripts at  
<http://www.hindawi.com>

